

# Role of the semi-lunar processes on jump dynamics in the locust

David Cofer<sup>+</sup>, Gennady Cymbalyuk<sup>§</sup>, William J. Heitler<sup>‡</sup>, and Donald H. Edwards<sup>\*</sup>

*Departments of Biology<sup>+</sup>, Physics and Astronomy<sup>§</sup>, and the Neuroscience Institute<sup>\*</sup>, Georgia State University, Atlanta, GA, 30303, USA, and the School of Biology, University of St. Andrews, St. Andrews, Fife, KY16 9TS, U.K.<sup>‡</sup>*

## Summary

The neural circuitry and biomechanics of kicking in locusts have been studied to understand their roles in the control of both kicking and jumping. It has been hypothesized that the same neural circuit and biomechanics governed both behaviors, but this hypothesis was not testable with current technology. We built a neuromechanical model to test this and to gain a better understanding of the role of the semi-lunar process (SLP) in jump dynamics. The SLP are highly sclerotized bands of cuticle that can be bent to store energy for use during kicking and jumping. High-speed video and mathematical analysis determined the amount of energy stored in the leg components. Previous work on kicking implied that the timing of unfurling may also be important. It has not been possible to directly test the affects of the SLP on jump performance because it is an integral part of the joint, and attempts to remove its influence prevent the locust from being able to jump. The jumping and kicking behaviors of the model were tested by comparing them to a variety of published data, and were found to reproduce the results from live animals. Tests compared the effects when the SLP was intact and disabled. The SLP significantly increased jump distance, power, total energy, and duration of the jump impulse. The geometry of the joint prevents the SLP from unfurling until the tibia has rotated beyond a threshold. This assists the flexor muscle and means it does not have to generate as much tension.

**Key words:** locust, semi-lunar process, jumping, kicking, biomechanics, Hill muscle model, muscle, neuromechanical simulation, model, neural circuit, invertebrate

## Introduction

The ability to escape predators is of great evolutionary importance. Many animals, including the locust, have evolved to specialize in jumping as a method of escape and locomotion. A common problem faced by all jumping animals is that while very rapid movements are required to propel the body, the ability to generate force in muscles decreases with the speed of muscle shortening. Consequently, it is difficult for muscle contraction to produce the larger forces required for high acceleration over the short time needed for escape. Locusts have evolved a specialization of the femur-tibia joint of their metathoracic legs that allow them to overcome this problem. On the distal end of each metathoracic femur, the locust has a highly sclerotized portion of cuticle that is called the semi-lunar process (SLP). The SLP bends like a bow to store energy that can later be used to power the jump (Bennet-Clark, 1975). This allows the locust to store energy in the SLP by a slow contraction of the powerful extensor muscle over a span of hundreds of milliseconds, and then later release that energy rapidly to power the jump.

The locust jump motor program consists of three phases (Burrows, 1995; Heitler and Burrows, 1977a). The first phase is cocking the leg. The locust prepares for a jump by activating the flexor tibia muscle to bring the tibia into a fully flexed position. The second phase is a period of co-contraction where both the extensor and flexor tibia muscles are active. The extensor tibia muscle slowly contracts and stores energy in the extensor apodeme, in the SLP, and in the leg cuticle. As tension builds in the flexor tibia, its distal tendon passes over a cuticular invagination in the ventral aspect of the distal ventral femur (Heitler's lump, Bennet-Clark, 1975). This enables the flexor tibia tendon to attach to the tibia at an angle of nearly  $90^\circ$  when the tibia is fully flexed, thereby maximizing its mechanical effectiveness in maintaining tibial flexion against the increasing tension in the much larger extensor tibia muscle (Heitler, 1974). The lump also acts as a catch or lock on the tendon that helps keep the tibia flexed while the flexor muscle has tension. In the third phase, the jump is triggered when both the flexor muscle and its motor neurons are inhibited. When the flexor tension drops below a threshold, the tendon slips off the catch and the tibia is rapidly extended to produce the jump (Heitler, 1974).

The function of the SLP during the jump has been inferred from its movement during kicks as recorded by high-speed video and from calculations of the energy stored in the extensor apodeme, the SLP, and femur cuticle (Bennet-Clark, 1975; Burrows and Morris, 2001). The energy stored in the SLP and the timing of its release appears to be important for jump performance. High-speed video of locusts kicks show that the SLP

does not begin unfurling until the tibia has rotated by more than 30° (Burrows and Morris, 2001). The reason for this delay, and the role it may play in the jump dynamics was unknown. Damage to the SLP, which is an integral part of the leg joint, makes the locust unable to jump, and so makes comparisons of the jump performance of animals with and without a functional SLP almost impossible.

In a similar manner, the motor circuitry responsible for the jump has been inferred from intracellular recordings from metathoracic neurons obtained during the kick, when the locust body is held stationary (Heitler, 1988; Heitler and Burrows, 1977a; Heitler and Burrows, 1977b). The similarity between the motor program responsible for the kick and the neuromuscular activity produced before and during the jump has led to the suggestion that the kick and jump motor programs are the same (Heitler and Burrows, 1977a). Technical limitations currently prevent an explicit test of this hypothesis.

The emerging field of neuromechanical simulation can help address these issues (Pearson et al., 2006). We have used a new neuromechanical simulator, AnimatLab ([www.Animatlab.com](http://www.Animatlab.com)), to build and test a model of the locust based on current descriptions of the neural and biomechanical processes that govern the jump. The model locust was then situated in a physically realistic environment within AnimatLab to study both the ability of the kick motor program to produce a realistic jump and the effects of the SLP on jumping behavior.

## Materials and Methods

### *Animals*

Adult locusts, *Shistocerca americana*, were obtained from a breeding colony at Agnes Scott College, kept caged in small groups at 37°C under a 12 hr L:D cycle, and fed fresh organic lettuce and 2/1 mixture of fresh wheat germ and powdered milk. Individuals were taken from the cage to a video-recording room and placed on a jumping platform. The platform contained a heating element that could adjust the local temperature and was covered by very fine sandpaper to allow the locust a slip-free surface for jumping. A 25x30 cm yellow wooden target was placed 30 cm from the platform, and jumps to the target were induced by either gentle touches of the abdomen by a hand-held wand or by raising the temperature of the platform. Animals were retrieved after the jump and returned to the platform for another attempt. Jumps were evoked at about 5 minute intervals; individuals were returned to their cage after 10 jumps. Locust jumps were

recorded at 500 fps and a resolution of 512x240 pixels by two Photron PIC R2 Fastcam video cameras with an exposure time of 0.5 ms.

### *Neuromechanical simulator*

AnimatLab is an open-source, freely available, Windows®-based software environment in which models of the body and nervous system of any jointed animal can be assembled and tested in a simulated physical world ([www.animatlab.com](http://www.animatlab.com)) (Cofer et al., 2009) (Reviewers: the site is currently password-protected until the cited paper is published. To access the site, go to: [www.animatlab.com/newdocs](http://www.animatlab.com/newdocs) and enter "animattester" for the user name and "animat" for the password. These instructions will be removed in the published text.). The model of an animal's body is created from a large variety of parts that are linked together through common elements such as joints, sensors, muscles and springs, and made to interact dynamically in a virtual physical world where all the relevant neural and physical parameters can be observed and manipulated. The model of the nervous system is constructed in a similar manner from a variety of parts that include single electrical compartment models that can represent either part or all of a neuron, electrical and chemical synapses, sensors, and muscles. The neural and body models are linked by identifying corresponding muscles and sensors in each model. The model is placed in a virtual physical world subject to gravity and surface friction. Stimuli (electrical currents or mechanical forces) can be applied to model elements to initiate action or to simulate an experiment, and the calculated responses, including membrane potentials, synaptic currents, forces, torques, and movements, can be displayed and recorded for additional analysis. These data are calculated and plotted simultaneously with the display of the model's movements in an interactive 3-D graphical animation.

### *Locust model*

To distinguish references to the model and its parts from references to the locust, the model part names have been given the italicized names of the corresponding locust body parts, while references to the locust and its body parts are made in normal font.

The 3-D graphical model of the *locust body* was developed from a 3-D polygon mesh that was purchased online ([www.turbosquid.com](http://www.turbosquid.com)) and then separated into individual *body segments* using the graphics program Blender ([www.blender.org](http://www.blender.org)). A polygon mesh is a set of vertices and triangular faces that define the volume for that segment. The dimensions of each segment were re-scaled to match published anatomical measurements

(Bennet-Clark, 1975; Heitler, 1974). All segments were assumed to have a uniform density, and the distribution of mass throughout the mesh volume determined the moment of inertia for that segment. The model has a body length of 48 mm and a total mass of 2.5 grams, with *metathoracic femur* and *tibia* lengths of 26 mm (Bennet-Clark, 1975). Individual body and limb segments were connected with either static or planar hinge joints in AnimatLab to assemble the locust body model. Angular limits on the hinge joints were set to restrict the movement of each joint to the normal range of the corresponding animal's joint. To ensure that the center of mass (COM) of the whole *locust* was located appropriately, small weighted masses were placed along the *body* axis of the *thorax* and *abdominal segments* to adjust the distribution of mass within the *body* (Bennet-Clark, 1975). The COM was then determined by pinning the *body* to a hinge joint and allowing it to rotate freely. Mass was re-distributed until the *locust* balanced both vertically and horizontally at the desired location. The locust model used for these simulations can be found at [www.animatlab.com/locust](http://www.animatlab.com/locust)

### *Biomechanics*

The geometry and biomechanical properties of the femur-tibia joint of the metathoracic leg play a crucial role in the energy storage for the jump (Fig. 1). The *tibia extensor muscle/apodeme* is shown as a red line that attaches to the *tibia* (Fig. 1a), while the *tibia flexor muscle/apodeme* is shown in blue. It wraps over *Heitler's lump* (Fig. 1h) and attaches to the *tibia* (Fig. 1c). The *femur* was connected to a small block of mass 1.6 mg that represented the *SLP* (Fig. 1f) (Bennet-Clark, 1975). A sliding prismatic joint connected the *SLP* to the *femur* (Fig. 1g). During normal co-contraction, the distal end of the *SLP* (where the *tibia* attaches) moves 0.3 mm ventrally and 0.4 mm proximally (Burrows and Morris, 2001). The slider joint was oriented to allow the *SLP* mass to move in the same direction (Fig. 1 b to g). A spring attached the *SLP* mass to the *femur* and was oriented along the direction of movement of the slider joint (Fig. 1e). The stiffness of the semi-lunar spring was calculated from a stress-strain curve obtained for the *SLP* (Bennet-Clark, 1975). Straining the process parallel to the extensor apodeme by 0.4 mm required approximately 14.2 N of force (Bennet-Clark, 1975). However, the semi-lunar process moves both proximally and ventrally, and this amount of proximal strain corresponds to 0.3 mm of ventral strain, for a total of 0.5 mm total strain. From this strain, we calculated

the stiffness of the SLP as 28.4 KN/m. The *semi-lunar* spring constant was set to this value.

The *tibia* was connected to the *SLP* mass by a hinge joint that allowed the *tibia* to rotate between 5° and 160° (Fig. 1b). The *femur-tibia* hinge joint is connected to the *SLP* mass, so that during co-contraction and *tibial* extension, the hinge joint will move along the slider with the *SLP* mass to approximate the joint movement observed in the locust (Burrows and Morris, 2001). The distances and angles that define the relationships between the *extensor* attachment, *femur-tibia* hinge joint, and *flexor* attachment were set to published measured values (ab is 0.76 mm, bc is 1.64 mm. Angle abc is 144°, and bcd is 143°) (Heitler, 1974).

Muscle is represented in AnimatLab by a linear Hill muscle model (Hill, 1970; McMahon, 1984; Shadmehr and Wise, 2005a; Shadmehr and Wise, 2005b). Each muscle model consists of a serial spring ( $K_{se}$ ) in series with the parallel combination of a parallel spring ( $K_{pe}$ ), a dashpot ( $B$ ), and a force actuator ( $T$ ). Muscle model properties are determined by the resting muscle length, the spring and dashpot constants, the stimulus-tension curve, and the length-tension curve. The stimulus-tension curve is a sigmoidal function that relates the force level of the actuator to muscle membrane depolarization. The length-tension curve is an inverse parabola that determines the percentage of actuator force that is applied at a given muscle length.

Only two muscles for each of the rear legs are modeled in this simulation, the flexor tibiae and extensor tibiae. The maximum force that can be produced by the extensor is 15 N, which is achieved upon depolarization after a latency of 300-800 ms (Bennet-Clark, 1975). The serial spring constant of the *extensor* was calculated using the Young's modulus of 18.9 kN.mm<sup>-2</sup> found for the extensor apodeme by Bennet-Clark (Bennet-Clark, 1975). The average size of the apodeme test pieces was 3 mm long x 0.25 mm wide x 40 um thick, and so they have an area of 0.01 mm<sup>2</sup>, and a length of 3 mm. These values allowed us to calculate the spring constant as 63 kN/m from Young's modulus using the equation  $K=YA/L$ , where  $Y$  is the modulus,  $A$  is the area, and  $L$  is the length. In the absence of published measurements that would allow calculation of the parallel spring constant, we used a value of 20 N/m because it produced a small but noticeable tension when the *extensor muscle* was stretched. The damping coefficient of the *extensor muscle* was set by hand to 700 Ns/m to produce a rise time to peak tension of approximately 400 ms. The stimulus-tension curve and the response properties of the non-spiking *neuron* that represents the muscle membrane were configured to reproduce the

twitch response of the extensor muscle to a single *FETi* spike at a femur-tibia angle of  $90^\circ$  (Heitler, 1988). The length-tension curve was also reproduced from muscle twitch values that were taken at various femur-tibia angles using direct stimulation of the muscle (Bennet-Clark, 1975). Direct stimulation of the *extensor muscle* produced twitch responses very similar to those recorded from extensor muscle in response to a *FETi* spike. The resulting length-tension curve of the *extensor muscle* reached the maximum at the fully flexed position and was reduced as the *leg* extended.

Recordings from the flexor muscle showed that it produces a maximum tension of around 0.75 N in response to tetanizing stimulation, and that it reached maximum tension 35-40 ms after a latency of 15 ms (Bennet-Clark, 1975). The following parameter values enabled the *flexor muscle* model to reproduce the recorded peak tension and tension time course: the serial spring constant,  $K_{se}$ , was 100 N/m, the parallel spring constant  $K_{pe}$  was 20 N/m, and the damping coefficient,  $B$ , was 10 Ns/m. The stimulus-tension curve was configured to produce the desired maximum tension. As with the *extensor* model, the *flexor* length-tension curve was near its maximum value when the *leg* was fully flexed and near its minimum value when the *leg* was extended.

The tendon on the flexor muscle of the locust contains a pocket. When the tibia is fully flexed and the flexor has a tension greater than 0.15 N, this pocket is caught on Heitler's lump, which helps keep the tendon locked in place (Bennet-Clark, 1975; Heitler, 1974). This tendon lock property plays an important role in the jump after co-contraction when the flexor muscle and motor neurons are being inhibited. The lock helps keep the tibia fully flexed even while the flexor tension is dropping. This prevents premature extension of the tibia and initiates the jump once the flexor tension drops below a threshold value for maintaining the lock. In the model, the tendon lock was represented by a spring that connects the *flexor attachment* to a point on the *femur* (Fig. 1, Magenta line between C and I). The spring was disabled and produced no tension unless the *tibia* was fully flexed and the *flexor* tension was greater than 0.15 N.

### *Neural Model*

A conductance-based, integrate-and-fire neuron model was used in this simulation. Neurons were modeled as a single equipotential compartment characterized by a set of user-specifiable parameters, including membrane time-constant, size (i.e., input conductance), membrane voltage, current noise, initial spike threshold, spike-frequency

accommodation, spike after-hyperpolarization conductance, and calcium conductances with activation and inactivation variables (MacGregor and Lewis, 1977).

The neural network used to generate both the *kick and jump motor programs* was designed to apply the correct motor signals in a sequence and duration that mimics the motor program seen during kicking in locusts (Heitler and Burrows, 1977a; Heitler and Burrows, 1977b). Initial flexion of the *tibia* begins when the nine *fast flexor tibia motor neurons* are stimulated to fire (Fig. 2a, Green *FLTi neurons*) (Burrows, 1995; Burrows, 1996). These neurons synapse onto the *flexor muscle membrane* (Fig. 2f, Light blue FM node) causing *muscle* depolarization and *flexor muscle* contraction. The *fast extensor of the tibia motor neuron* (Fig. 2b, Red *FETi neuron*) synapses onto the *extensor muscle membrane* (Fig. 2e, Light blue EM node) causing it to contract. A central excitatory *synapse* connects the *FETi neuron* to the *fast flexor motor neurons* (b to a) (Burrows, 1996; Heitler and Burrows, 1977b). There are also two *inhibitory interneurons* that are involved in triggering the jump. The multimodal '*M*' *interneuron* (Fig. 2c, Gold *M neuron*) inhibits the excitatory *flexor motor neurons*, while the inhibitory *flexor inhibitor motor neuron* (Fig. 2d, Yellow *FI neuron*) *synapses* onto the *flexor muscle* and inhibits it directly (Burrows, 1995; Pearson et al., 1980). The *Tendon Lock control node* (Fig. 2g, Light blue) is responsible for enabling the tendon lock spring when the *tibia* is sufficiently flexed and the *flexor* has a tension above the lock threshold. The network that governs the right *metathoracic leg* is shown in Fig. 2; an identical network, also excited by the same *Flexion Command neuron*, governs the left *metathoracic leg*.

*Neurons* were configured to reproduce the observed firing frequencies. Peak *FETi* neuron firing ranged between 60-100 Hz (Heitler and Burrows, 1977a), while the *FLTi* neurons fired around 60 Hz (Heitler and Burrows, 1977a). The central *excitatory synapse* connecting the *FETi* to the *FLTi neurons* was configured by reproducing an experiment in which the *FETi* was stimulated to fire at roughly 10 Hz while the *synaptic response* of the *FLTi* was monitored (Heitler and Burrows, 1977b). The first *FETi spike* produced a 20 mV *EPSP* in all of the *FLTi motoneurons*; the *EPSPs* decayed in approximately 100 ms (Burrows, 1996; Heitler and Burrows, 1977b). Responses to subsequent *spikes* were reduced by *synaptic depression* in a manner similar to that observed experimentally (Heitler and Burrows, 1977b).

All *neurons* had a random tonic noise of 0.3 mV added to their *membrane potentials* at each time step. The pseudo-random number generator that controlled the noise was initialized using a random seed value at the beginning of each simulation. This caused

each simulation with a different seed to produce slightly different results because changes in the *neuron* voltages led to alterations in the timing of the *motor program* and the rise and fall times of the tension in each of the *muscles*. To compare the effects of differences in model parameters on performance, the same seed value of the random number generator was used to create the same initial conditions for simulations with both models.

### *Procedures for Simulation of Experiments*

During the *kick* simulations, the *locust* was suspended above the *ground* and rotated so that its ventral surface was uppermost, and pinned in place so it could not fall. All *leg joints* except the *femur-tibia* and *tibia-tarsus joints* of the *metathoracic legs* were locked to prevent rotation. The *kick motor program* caused the *tibia* to flex initially and then kick out at high speed. This allowed us to measure the movement of the *SLP* and *tibial* rotation. *SLP* torque relative to the *extensor attachment* was calculated by recording the coordinates of the *femur-tibia joint*, *extensor attachment*, and the *SLP* force vector. These values were used to calculate the moment arm of the *SLP* force vector relative to the *extensor attachment*, and this was used to calculate the torque applied by the *SLP*. *Kick* velocity was measured as the peak velocity between the beginning of the *kick* and end of the *kick* when the *tibia* had fully rotated by  $160^\circ$ . *Kick* duration was the time from the beginning of the *kick* till full rotation of the *tibia*.

Simulations of the locust jump began with the *locust* held 4.5 cm above the *ground*, and then dropped to the *ground*. Initially, only the *coxa-femur joints* of the *rear legs* were free to rotate. All other *joints* were locked and unmoving. After the *locust* came to rest, the other *joints* in the *rear leg* were unlocked so that the *motor program* could proceed. Once the *tibia* was fully flexed, the *metathoracic coxa-femur joint* was adjusted to fix the angle of the *leg* with respect to the *ground* at  $45^\circ$ . The *joints* for all the other *legs* remained locked throughout the *jump motor program* in order to maintain a stable and consistent posture, and the posture of the *front legs* was adjusted to fix the initial *body pitch* of the *animal* at  $3^\circ$ . The locks on the *joints* of the *front* and *middle legs* were disabled when the *jump* was triggered. This allowed all the *legs* to move freely throughout the take-off and ballistic phase of the jump. The *SLP* was disabled for tests by locking the *SLP* sliding prismatic joint to prevent it from moving and by disabling the *SLP* spring to prevent it from generating tension. The maximum tension in the *extensor tibia muscle* was varied by adjusting the maximum tension that the *muscle* could generate.

Power for the *jump* was calculated using the same method outlined in Bennet-Clark (Bennet-Clark, 1975). The force acting on the *body* during the *jump* impulse was multiplied as the dot product of the velocity vector acting on the *body* to obtain the power. Energy was calculated by integrating the power curve over the time period of the impulse. The same stimulus pattern that was used for *kicks* was applied to produce the motor pattern for the *jump*. *Jump* distance was measured using the position of the *locust* at the beginning of the *jump* and when either the *body* or one of the rear *legs* first touched the *ground*. The beginning of a *jump* or *kick* was always measured from when the tendon lock was disengaged. *Jump* duration was the time from the beginning till the end of the *jump*. *Jump* impulse duration was the time from the beginning of the *jump* until one of the *legs* lost contact with the *ground*. *Jump* velocity and acceleration was the peak of those values obtained during the *jump* impulse. All data analysis was performed in Matlab (Matlab R2007a, Mathworks Inc.), and statistical comparisons were made using its Anova1 one-way analysis of variance function.

The influence of *SLP* flexion torque on the *flexor muscle* was determined by comparing the tension level at which the *extensor muscle* was able to overcome the tension in the *flexor* when the *SLP spring* was intact and when it was disabled. The *extensor* tension was set to 5 N and the *tendon lock* was disabled for both tests. The first test was performed with the *SLP* intact, while in the second test the *SLP spring* was disabled. Once the *extensor* reached the 5 N tension level the *flexor* was inhibited and its tension dropped until it reached a point where the *extensor muscle* was able to overcome it and extend the *leg*.

## Results

The simulated motor program and patterns of *muscle* activity responsible for the *kick* are shown in Fig. 3. The *kick motor program* began by stimulating the nine *FLTi* motoneurons on the right and left side to fire at about 60 Hz, which produced tension in the *flexor muscles* that caused the left and right *tibiae* to become fully flexed (Fig. 3a and f). A train of current stimuli applied to the *FETi* motoneurons on both sides began the co-contraction phase (Fig. 3b and e). Each current stimulus evoked a corresponding spike in *FETi*. In addition to driving the *extensor muscle*, the *FETi* excited the *FLTi*s on the same side (Heitler, 1988) to enable the *flexor muscle* to keep the *tibia* flexed despite the mounting *extensor* tension. The kick was triggered by direct stimulation of the *FI* (Fig.

3d) and *M inhibitory neurons* (Fig. 3c) with an applied current for 80 ms, which caused them to fire at approximately 200 Hz. The *FI neuron* directly inhibited the *flexor muscle*, causing the *flexor* tension to decline rapidly. Simultaneously, the *M neuron* inhibited the *FLTs* to remove the drive on the flexor muscle. Rapid inhibition of the *FLTs* and the *flexor muscle* triggered the kick by reducing the *flexor* tension below the level needed to maintain the *tendon lock* (Fig. 3f and g) (Heitler and Burrows, 1977a; Pearson et al., 1980). With the *flexor tendon lock* disabled, the *tibia* began to extend very rapidly, completing extension in 5 ms, the same time-course that was recorded with high-speed videography (Burrows and Morris, 2001).

To test the hypothesis that the same neural circuitry and motor program could produce both the kick and the jump, we used the model of the kick circuit and motor program to evoke a simulated jump. An expanded view of the data for both the kick and jump are shown in Fig. 4. Although the same motor program controlled both simulated behaviors, the unloaded *leg* extended in less than 5 ms to produce the *kick* (Fig. 4A), whereas the load imposed by the *body* caused the *leg* to extend much more gradually to produce the *jump* (Fig. 4B). Comparison of the simulated movements of the *locust* with a series of frames taken of a locust's jump (*Shistocerca americana*) by a high-speed camera operating at 500 fps (Fig. 5) shows that the simulation has captured the most salient features of the resulting jump behavior.

Published measures of locust (*Shistocerca gregaria*) jump behavior (Table 1) provide benchmarks with which to compare the model *locust* jump behavior. Model *locust* jumps were performed with randomly seeded noise added to the *membrane potentials* of all the model *neurons* and *muscles*, while all other model parameters were kept constant. Randomly seeded membrane potential noise ensured that the *locust* behaved slightly differently for each jump due solely to the randomness in the neurons and their affect on the biomechanics, and this provided a method to measure the variance of the *behavior* when all other initial conditions were identical. Several indicators of *jump* performance were measured, compared to the published benchmark values for live locusts (Table 1), and found to be essentially the same. This similarity demonstrates that the jump performance of the *locust* using the kick motor program closely matched that of the live locusts.

The contribution of the *SLP* to the *locust* jump was analyzed by comparing jumps made with the *SLP* intact to jumps made with it disabled. The *extensor* tension was varied from 7 to 15 N in steps of 2 N. For all *extensor* tension levels tested there was a

significant reduction in the distance *jumped* when the *SLP* was disabled (Fig. 6A). The average percentage difference in *jump* distance was  $37.3 \pm 5\%$  at the maximum tension of 15 N, and this decreased to  $24.8 \pm 5.8\%$  at 7 N (Fig. 6B). The peak power of the *jump* impulse when the *SLP* was intact was significantly higher than when the *SLP* was disabled ( $2.04 \pm 0.07$  with,  $1.28 \pm 0.07$  mW without,  $p < 10^{-30}$ ; Fig. 7A). A higher peak power also resulted in a significant increase in the total energy for the *jump* ( $16 \pm 0.6 \cdot 10^{-3}$  with,  $9.9 \pm 0.4 \cdot 10^{-3}$  mJ without,  $p < 10^{-30}$ ). In addition, when the *SLP* was disabled, the power ended significantly sooner than it did when the *SLP* was intact ( $22.8 \pm 0.27 \cdot 10^{-3}$  with,  $22.3 \pm 0.34 \cdot 10^{-3}$  ms without,  $p < 10^{-5}$ ). The percentage difference between the two *jumps* in this pair were calculated, and then the average and standard deviation of all pairs was determined (Fig. 7B). This showed that the average percentage difference in *jump* power remained just below 40% throughout most of the *jump* impulse. Near the end it rose quickly because the power for the *jump* without the *SLP* fell sooner than when the *SLP* was intact.

High-speed video of locust kicks have shown that the *SLP* does not unfurl until after the tibia has extended by more than  $30^\circ$  degrees (Burrows and Morris, 2001). To analyze this result through simulations, the locust kick was reproduced by the *locust*. Fig. 8A shows the amount of strain of the *SLP* plotted with the *FT joint* rotation against the time of the *jump*. The filled black squares mark the values of the *SLP* strain at 1 ms intervals as would be recorded by a high-speed video camera operating at 1000 fps, like those reported in Fig. 3B of Burrows and Morris (2001). Dashed line 2 is the first instance where a significant unfurling of the *SLP* would be detected at 1000 fps, and this corresponds to a *FT* rotation of  $38.12^\circ$ . In order to understand what caused this delay it is useful to look at the *SLP* torque (Fig. 8B), which was generated by the *SLP* force relative to the *extensor* attachment. At the beginning of the *kick*, with the *tibia* still flexed, the *SLP* torque was negative, and acted to keep the *leg* flexed (Fig. 8C). Moreover, the tension in the *extensor apodeme* kept the *SLP* contracted. When the negative torque produced by the *flexor muscle* was removed by inhibition, the positive torque exerted by the *extensor muscle* began to extend the *leg*. The *extensor attachment* was pulled through the *SLP* force vector, causing the negative flexion *SLP* torque to decrease and change to a positive extension torque (Fig. 8C). In that position, the *SLP* torque enhanced the *femoral-tibia joint* rotation, and the *extensor* tension could no longer prevent it from unfurling. After the torque became positive, the strain in the *SLP* rapidly decreased. Prior to this time (dashed line 1), the strain had decreased by less than 10%.

The effect of the *SLP flexion* torque on the *flexor muscle* was determined by comparing the amount of *flexor* tension that was required to keep the *leg* in a fully flexed position when the *SLP spring* was intact and when it was disabled. When the *SLP spring* was intact the *flexor muscle* was able to hold the *tibia* in a fully flexed position until the tension dropped to a minimum of 0.26 N. When the *SLP spring* was disabled then flexion torque generated by the *SLP* was removed and the minimum *flexor* tension required to keep the *leg* from extending rose to a value of 0.56 N. When the *SLP spring* was present it required 54% less tension in the *flexor muscle* to keep the *leg* from extending when the *tibia lock* was not active.

## Discussion

The neural control and biomechanics of locust kicking have been well described because the kick can be elicited while the locust is dissected and restrained, thus allowing simultaneous intracellular recordings from neurons in the ganglia and EMG in the muscles. Although it is currently not possible to make these recordings in a jumping locust, the similarities between the kick and jump have led to the assumption that the same motor program may produce both behaviors. A virtual neuromechanical model of the locust has allowed us to determine whether the neural circuit, motor program, and biomechanical configuration of the locust legs are sufficient to account for the jump as well as the kick. Our results demonstrate that the kick motor program is capable of reproducing the full range of jump behaviors that have been described in the literature, and that the control of the key variable of extensor tension gives the locust the ability to alter important jump variables like the jump distance, and take-off velocity. These results strongly support the hypothesis that the kick motor program is used for both kicking and jumping.

The locust jump is an important behavior of locusts for both locomotion and escape from predators. The SLP is an evolutionary adaptation that has been thought to allow locusts to jump significantly farther than they could without it. However, because of the biomechanics of the metathoracic FT joint, direct tests of the effects of the SLP on jump performance of live locusts are difficult or impossible. The neuromechanical model of a locust presented here has allowed us to identify the contributions that the SLP makes to the jump. The simulations indicate that the SLP can act first to help keep the leg flexed

until the rotation of the tibia changes the sign of the SLP torque to favor extension. They also showed how the *SLP* increased the power by almost 40% throughout most of the *jump*.

The primary role of the flexor muscle of the metathoracic leg during jumping and kicking is to keep the tibia in a fully flexed position while co-contraction is occurring. The flexor muscle must be big enough to carry out this role, but any excess volume devoted to the flexor muscle is wasteful and that volume would be better used by the extensor muscle to provide more power for the jump. When the *SLP spring* was disabled any flexion torque that it generated was removed, and it took 54% more *flexor* tension to keep the *tibia* from extending. The flexion torque generated by the *SLP* was able to assist the *flexor muscle* and help keep the *tibia* flexed. This meant that the flexor could be less powerful, and thus more volume could be devoted to the extensor muscle.

High speed video of locust kicking has shown that unfurling of the SLP is delayed until after the tibia had rotated by greater than 30° (Burrows and Morris, 2001). The locust model helps to explain why there is a delay in the unfurling of the SLP, and how this affects the jump abilities of locust. As shown in Fig. 7, the delay appears to depend on the movement of the *extensor tibiae* attachment point through the *SLP* force vector, changing an *SLP* torque that produced flexion to one that promotes *leg* extension. Finally, the simulations show that the *SLP* enables the *locust* to *jump* between 25% and 40% farther than without it, depending on the force applied by the *extensor tibia*.

Storing energy using deformation of cuticle or strain in apodemes are common methods of overcoming the limitations of skeletal muscle that is required for arthropods to make quick movements like jumping and snapping. Some of these animals have evolved elaborate specializations to allow them to perform these rapid movements. The rabbit flea *Spilopsyllus cuniculus* stores energy for its jump in a resilin pad in the internal skeleton of its thorax. The energy is quickly released by the contraction of a small muscle that shifts the point of action of the depressor muscle, allowing the femur to be depressed (Bennet-Clark and Lucey, 1967). The froghopper, *Philaenus spumarius*, stores energy for the jump by bending a bow-like cuticle formation in the pleural arch. A friction locking system prevents the legs from moving until tension in the depressors exceeds the holding force of the lock (Burrows, 2003; Burrows, 2006; Burrows et al., 2008). Both the trap-jaw ant, *Odontomachus*, and the snapping shrimp, *Alpheus californiensis*, store energy for the rapid closing of their mandible or claw in the apodeme of the muscle and by deformation of the cuticle of the exoskeleton (Gronenberg, 1995a; Gronenberg, 1995b; Ritzmann,

1973). While all these mechanisms are similar, there is a difference that appears to be unique to the SLP mechanism of the locust. Energy from the jump primarily comes from the apodeme of the extensor and the SLP. Unlike the case with the resilin pad in the flea and pleural arches in the frog hopper, the SLP and apodeme both produce forces that are on very different directions in the locust, and this is a key feature for causing the delay in unfurling the SLP.

This work demonstrates the utility of neuromechanical simulation for analysis of the interaction of neural mechanisms of control with biomechanical processes that mediate and constrain the animal's movement. Neuromechanical simulation enables the operation of neural circuits that have been described in dissected, restrained and anesthetized animals to be understood in something like their natural context, where the consequences for movement of their activity become readily apparent.

### Acknowledgements

We wish to acknowledge support for this work from National Science Foundation research grant 0641326 to DHE; from a Brains & Behavior Seed Grant from Georgia State University, from the Brains & Behavior Fellowship Program at Georgia State University, and from National Institutes of Health exploratory grant GM065762. We would also like to thank Dr. Karen Thompson of Agnes Scott College for supplying us with locusts for testing, and for instructing us on their maintenance and care.

### References

- Bennet-Clark, H. C.** (1975). The energetics of the jump of the locust *Schistocerca gregaria*. *J Exp Biol* **63**, 53-83.
- Bennet-Clark, H. C. and Lucey, E. C.** (1967). The jump of the flea: a study of the energetics and a model of the mechanism. *J Exp Biol* **47**, 59-67.
- Burrows, M.** (1995). Motor patterns during kicking movements in the locust. *J Comp Physiol [A]* **176**, 289-305.
- Burrows, M.** (1996). *The Neurobiology of an Insect Brain*. Oxford: Oxford University Press.
- Burrows, M.** (2003). Biomechanics: frog hopper insects leap to new heights. *Nature* **424**, 509.
- Burrows, M.** (2006). Morphology and action of the hind leg joints controlling jumping in frog hopper insects. *J Exp Biol* **209**, 4622-37.
- Burrows, M. and Morris, G.** (2001). The kinematics and neural control of high-speed kicking movements in the locust. *J Exp Biol* **204**, 3471-81.
- Burrows, M., Shaw, S. R. and Sutton, G. P.** (2008). Resilin and chitinous cuticle form a composite structure for energy storage in jumping by frog hopper insects. *BMC Biol* **6**, 41.

- Cofer, D. W., Cymbalyuk, G., Reid, J., Zhu, Y., Heitler, W. and Edwards, D. H.** (2009). AnimatLab: A 3-D graphics environment for neuromechanical simulations. *Manuscript submitted for publication in J. of Neuroscience Methods*.
- Gronenberg, W.** (1995a). The fast mandible strike in the trap-jaw ant *Odontomachus* I. Temporal properties and morphological characteristics. *J Comp Physiol A* **176**, 391-398.
- Gronenberg, W.** (1995b). The fast mandible strike in the trap-jaw ant *Odontomachus* II. Motor control. *J Comp Physiol A* **176**, 399-408.
- Heitler, W.** (1974). The locust jump. Specialisations of the metathoracic femoral-tibia joint *J Comp Physiol* **89**, 93-104.
- Heitler, W.** (1988). The role of fast extensor motor activity in the locust kick reconsidered. *J Exp Biol* **136**, 289-309.
- Heitler, W. J. and Burrows, M.** (1977a). The locust jump. I. The motor programme. *J Exp Biol* **66**, 203-19.
- Heitler, W. J. and Burrows, M.** (1977b). The locust jump. II. Neural circuits of the motor programme. *J Exp Biol* **66**, 221-41.
- Hill, A. V.** (1970). First and last experiments in muscle mechanics. Cambridge: Cambridge University Press.
- MacGregor, R. and Lewis, E.** (1977). Neural Modeling: Electrical Signal Processing in the Nervous System. New York: Plenum Press.
- McMahon, T. A.** (1984). Muscles, reflexes, and locomotion. New Jersey: Princeton University Press.
- Pearson, K., Ekeberg, O. and Buschges, A.** (2006). Assessing sensory function in locomotor systems using neuro-mechanical simulations. *Trends Neurosci* **29**, 625-31.
- Pearson, K. G., Heitler, W. J. and Steeves, J. D.** (1980). Triggering of locust jump by multimodal inhibitory interneurons. *J Neurophysiol* **43**, 257-78.
- Ritzmann, R.** (1973). Snapping Behavior of the Shrimp *Alpheus californiensis*. *Science* **181**, 459-460.
- Shadmehr, R. and Wise, S.** (2005a). Computational Neurobiology of Reaching and Pointing: A Foundation for Motor Learning. Cambridge, MA: MIT Press.
- Shadmehr, R. and Wise, S.** (2005b). A simple muscle model. Supplement to (Shadmehr and Wise, 2005a). Online at <http://www.shadmehrlab.org/book/musclemodel.pdf>.

## Figures

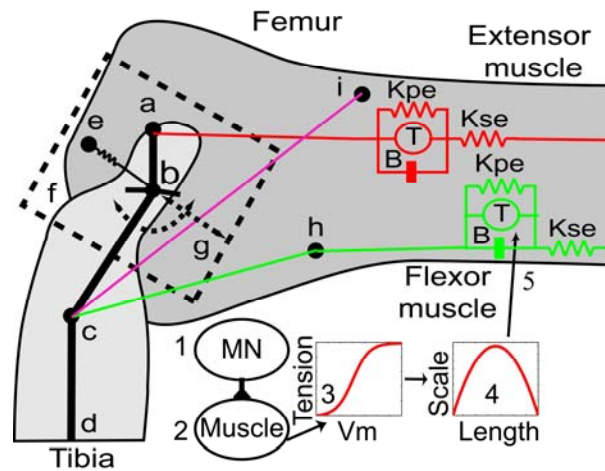


**Figure 1. Model of the femur-tibia (FT) joint of the metathoracic leg.** (a) Extensor apodeme attachment point on the tibia. (b) FT hinge joint and connection of SLP spring. (c) Flexor apodeme attachment point on the tibia. (d) A point further down tibia. (e) The SLP spring is attached between the femur and the tibia. (f) The SLP mass moves along the slider joint (g) oriented between the points b and g that is at an inclination of  $36.9^\circ$ . (h) Heitler's lump. The flexor muscle wraps over this lump to alter its orientation with respect to the tibia as the leg is moved. (i) The tendon lock is modeled as a spring located between points c and i. It is only enabled when the tibia is fully flexed and flexor muscle has a tension greater than 0.15 N (Bennet-Clark, 1975; Heitler, 1974). The distance between ab is 0.76 mm, bc is 1.64 mm. The angle abc is  $144^\circ$ , and bcd is  $143^\circ$  (Heitler, 1974). The muscle model is shown for the flexor and extensor muscles. This consists of a spring (Kpe) in parallel with a tension generator (T), and a dashpot (B), in series with another spring (Kse). (1) The muscle is activated by firing of a motor neuron (MN). (2) This depolarizes the muscle membrane. (3) Changes in the membrane voltage are converted to a tension value using a sigmoidal function. (4) The tension value is scaled based on the muscle length. (5) The scaled tension is applied to the muscle in the force generator producing a contraction.

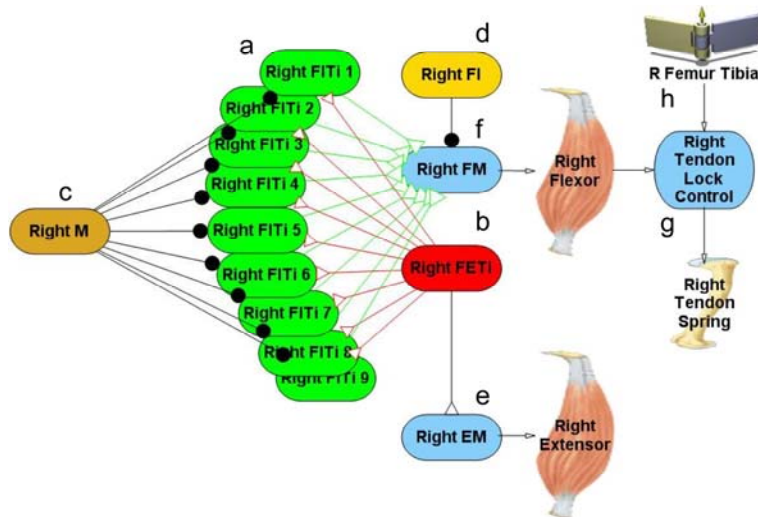


**Figure 2. Neural network model of the *jump* motor program.** Network shown is for the right leg. **(a)** Nine *fast flexor tibia motor neurons* (Green *FITi*). *FITi*s synapse onto the *flexor muscle membrane* (Light blue *FM*). **(b)** A single *fast extensor tibia motor neuron* (Red *FETi*). *FETi* synapses onto the *extensor muscle membrane* (Light blue *EM*). **(c)** The *multimodal interneuron* (Gold *M*) inhibits the *FITi*s. **(d)** The *flexor inhibitor* (Yellow *FI*) directly inhibits the *flexor muscle*. **(e)** Depolarization of the *extensor muscle membrane* causes the *extensor muscle* to contract. **(f)** Depolarization of the *flexor muscle membrane* causes the *flexor muscle* to contract. **(g)** The *tendon lock control* node (Light Blue) controls when the *tendon lock spring* is enabled based on the rotation of the *tibia* and the tension in the *flexor muscle*. **(h)** When the *jump* is triggered the *femur-tibia* joint rotates rapidly to produce the *jump* or *kick*.

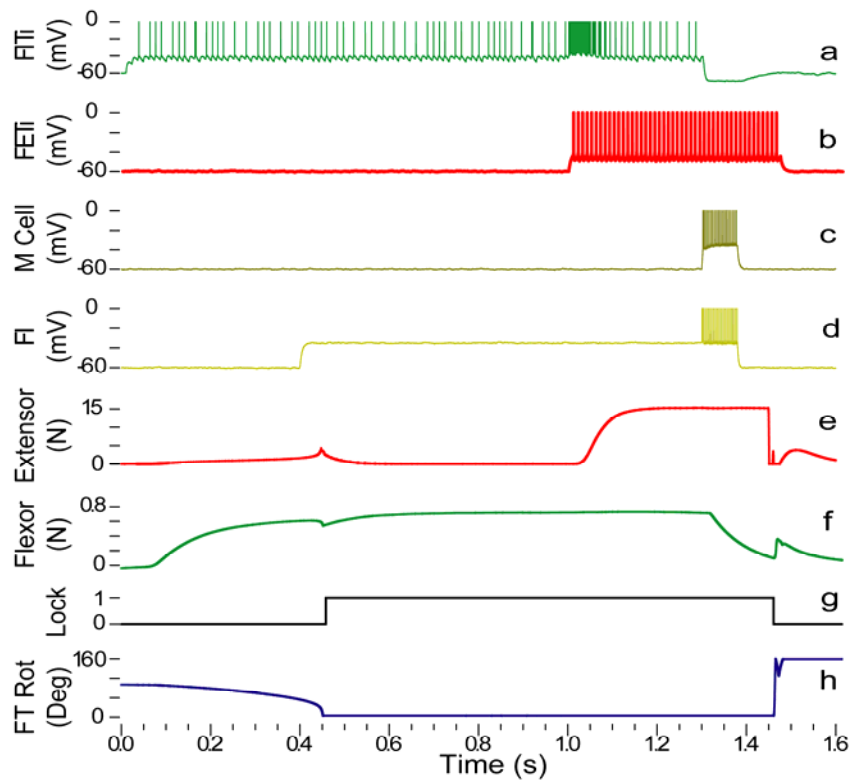


**Figure 3. Neural output of the jump motor network.** The nine flexor motor neurons were stimulated to fire (**a**) during the cocking phase and rotated the tibia into a fully flexed position. The extensor motor neuron FETi (**b**) began firing during co-contraction and the central excitatory synaptic connection from FETi to FLTi caused a brief increase in flexor frequency. The inhibitory interneurons M (**c**) and FI (**d**) then began firing once the extensor had reached the desired tension level (**e**). This caused the tension in the flexor (**f**) to fall below the threshold of the tendon lock (**g**) and this disabled the tendon spring. This produced a rapid extension of the tibia (**h**). Each chart corresponds to the output from a labeled element from figure 2.

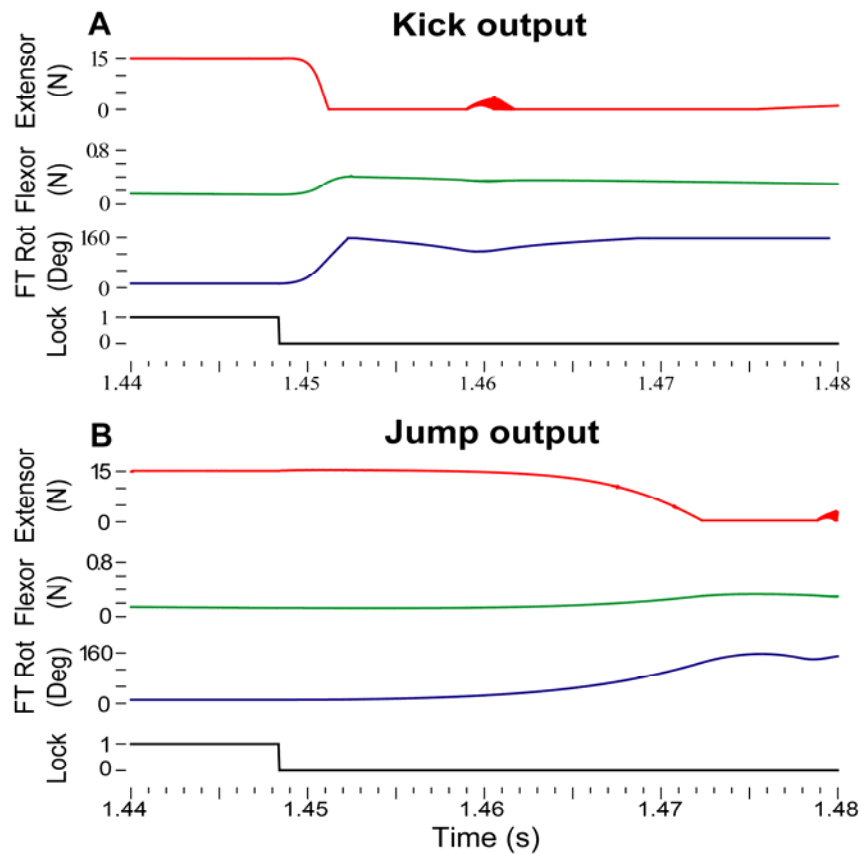


**Figure 4. Expanded view of *jump* or *kick* data.** *Kick* data from fig. 3 is expanded and compared to data from a *jump*. The output of the motor program was the same for both the *kick* and the *jump* so it was omitted here. Each chart shows the tension in the *extensor* and *flexor* muscle of the *left metathoracic leg*, the rotation of the *FT joint*, and the status of the *tendon lock*. **(A)** To produce a *kick*, the *tibia* began to rotate very rapidly after the *tendon lock* was disabled, and completed full extension in 4.1 ms. **(B)** The *jump* used the same motor program, but the *leg* rotated more slowly because the *tibia* was loaded, and so reached its maximum value after 28.35 ms.

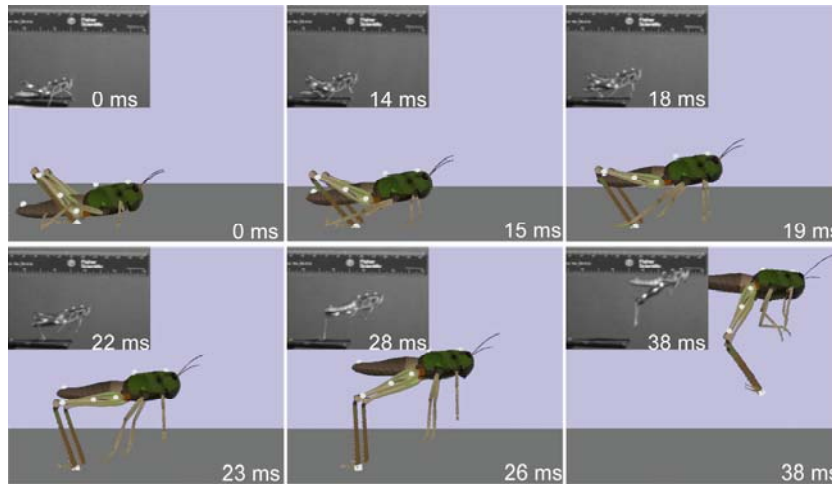


**Figure 5. Screenshots of the simulated and real locust jumping.** Images of a real locust jump are in the insets. The simulated locust produces a jump very similar to those recorded from live locusts. Live locust images are sequential frames taken using a high speed camera at 500 fps.

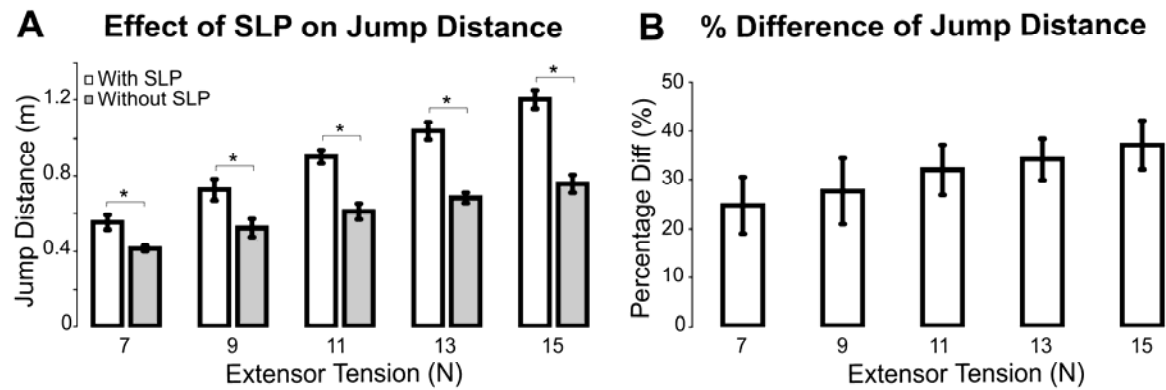


**Figure 6. Effect of *SLP* on *jump* distance.** (A) Jumps were performed with and without the *SLP* for a variety of different *extensor* tension values. At all values tested there was a significant difference between the distance *jumped* with and without the *SLP*. ( $p < 10^{-13}$ ) (B) The percentage difference for the maximum *extensor* tension value of 15 N was  $37.3 \pm 5$  percent, and this value declined slightly for decreasing values of *extensor* tension. Each test was performed with an  $N=20$ .

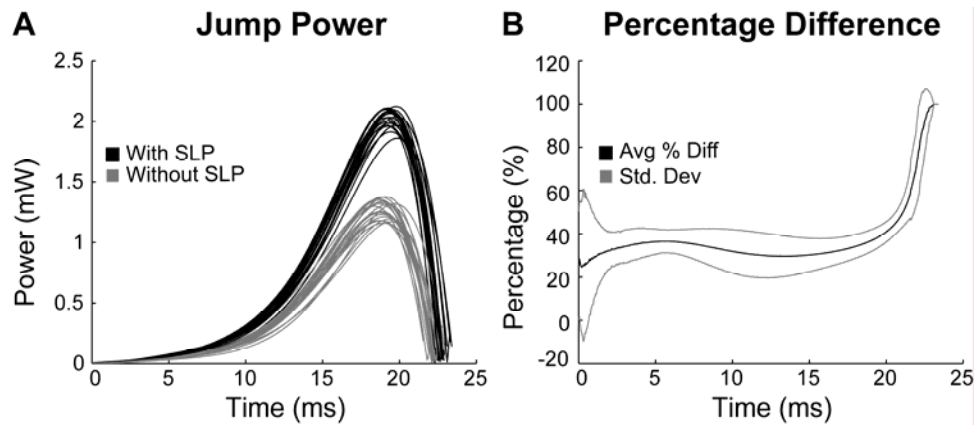


**Figure 7. Jump power with and without SLP.** Extensor tension is at 15 N. **(A)** Jump power with the SLP intact (black) and with the SLP disabled (grey). There is a significant difference in the magnitude of the peak power ( $2.04 \pm 0.07$  with,  $1.28 \pm 0.07$  mW without,  $p < 10^{-30}$ ), the total energy during the *jump* impulse ( $16 \pm 0.6 \cdot 10^{-3}$  with,  $9.9 \pm 0.4 \cdot 10^{-3}$  mJ without,  $p < 10^{-30}$ ), and the duration of the impulse ( $22.8 \pm 0.27 \cdot 10^{-3}$  with,  $22.3 \pm 0.34 \cdot 10^{-3}$  ms without,  $p < 10^{-5}$ ). **(B)** The percentage difference for each pair of *jumps* with and without the SLP was calculated and averaged. The average percent difference between the two *jumps* remained steady near 40% for most of the duration of the *jump* impulse and then increased near the end because the power without the SLP dropped off more quickly than when the SLP was intact.

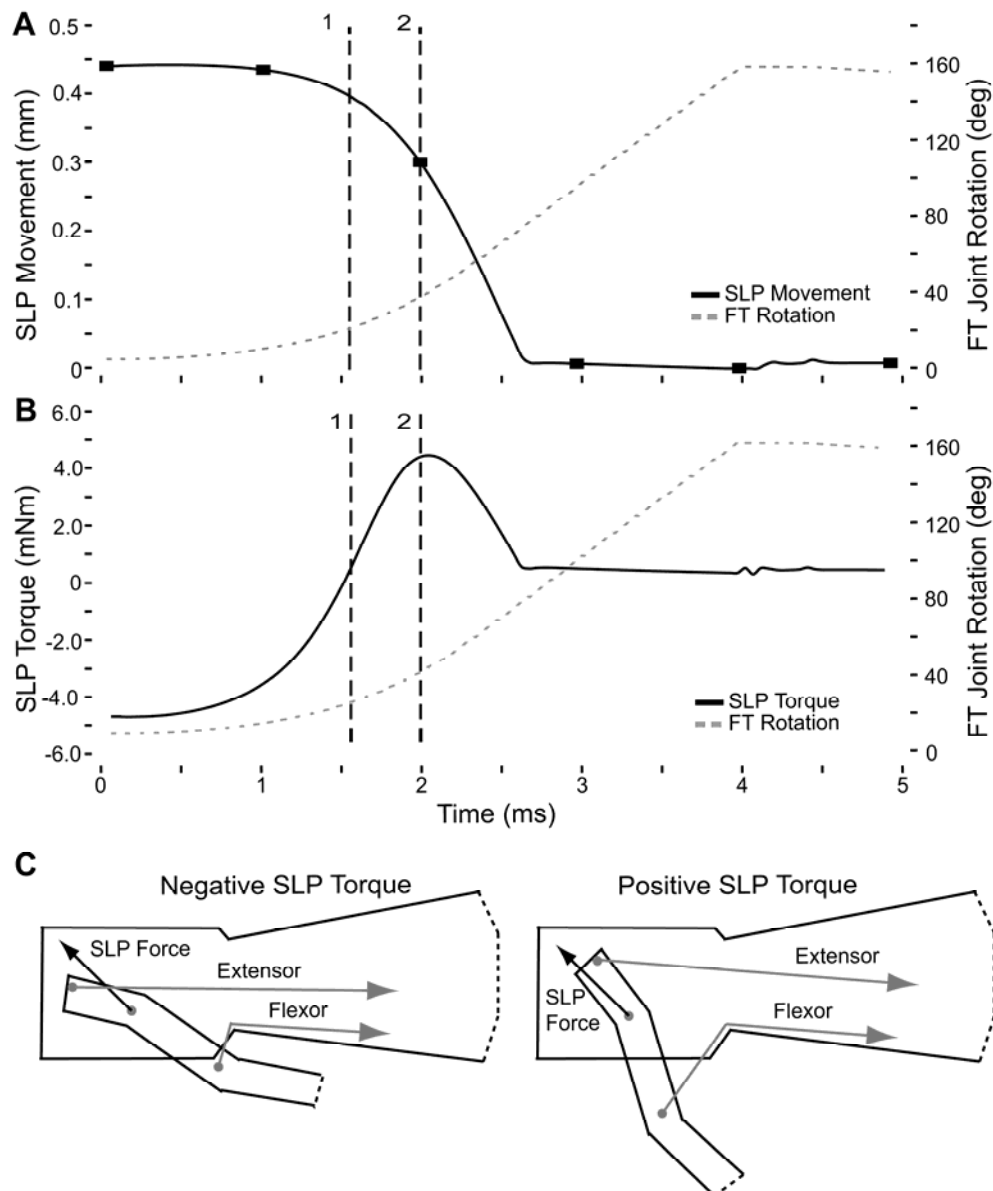


**Figure 8. SLP movement and torque during a kick.** Data was taken from the left *metathoracic leg* at an *extensor* tension of 15 N. **(A)** SLP movement is the black solid line with its axis on the left side, while the rotation of the *femur-tibia joint* is the grey dashed line with an axis on the right. The *FT joint* rotated with a maximum velocity of  $63^{\circ}\text{ms}^{-1}$  and took 4 ms to reach its full extension of  $160^{\circ}$ . The SLP began with a strain of 0.447 mm and rapidly unfurled during the *kick*. The filled black squares represent the values at 1 ms time intervals where a high speed camera at 1000 fps would take images to provide a comparison with the plot Fig. 3B of (Burrows and Morris, 2001). The first point where a noticeable decrease in the SLP would be visible at 1000 fps is shown with the line (2). This corresponds to a *FT* rotation of  $38.12^{\circ}$ . **(B)** SLP torque is the black solid line with its axis on the left side, while *FT* rotation is again shown in dashed grey on the right side. SLP torque is the torque generated solely by the SLP force relative to the *extensor* attachment point. The torque started negative and this helped prevent the SLP

from unfurling. It was only after the torque became positive that significant and rapid unfurling occurred. This time is shown at dashed line (1). Before this time the *SLP* unfurled less than 10%, while immediately afterwards the rest of the unfurling occurred. (C) Negative *SLP* torque occurred when the force applied by the *SLP* caused torques that retarded *tibia* rotation, while positive torque enhanced *tibia* rotation. Positive torque only occurred after the *leg* had rotated enough to move the *extensor* attachment point to the opposite side of the *SLP* force vector.

| <b>Measure</b>        | <b>Units</b>        | <b>5 N</b>  | <b>8 N</b>  | <b>15 N</b> | <b>Experimental</b>    |
|-----------------------|---------------------|-------------|-------------|-------------|------------------------|
| Jump Distance         | (m)                 | 0.34±0.013  | 0.62±0.033  | 1.122±0.268 | 0.5-0.7 <sup>1</sup>   |
| Jump Duration         | (s)                 | 0.33±0.027  | 0.458±0.041 | 0.587±0.142 | 0.31-0.43 <sup>1</sup> |
| Jump Impulse Duration | (ms)                | 51.4±0.6    | 35.3±0.34   | 23.5±5.5    | 25-30 <sup>1</sup>     |
| Jump Velocity         | (m/s)               | 1.8±0.117   | 2.51±0.054  | 3.6±0.07    | 2.2-3.2 <sup>1</sup>   |
| Jump Acceleration     | (m/s <sup>2</sup> ) | 104±6       | 176±6.7     | 290±6.6     | 180 <sup>1</sup>       |
| Peak Jump Power       | (mW)                | 0.371±0.038 | 0.87±0.04   | 2.04±0.08   | 0.75 <sup>1</sup>      |
| Jump Energy           | (mJ)                | 4±0.46      | 7.8±0.33    | 16±0.44     | 14 <sup>1*</sup>       |
| Kick Velocity         | (deg/ms)            | 34.47±0.1   | 44.3±0.134  | 62.58±0.145 | 54.5±1.3 <sup>2</sup>  |
| Kick Duration         | (ms)                | 8.41±0.018  | 5.96±0.02   | 4.1±0.01    | 3-6 <sup>2</sup>       |

**Table 1. Comparison of real and simulated locust jump performance.** A number of key parameters of the virtual locust jump were compared with values published in the literature for live locusts. Simulations were performed using three different *extensor* tension values at 5, 8, and 15 N to demonstrate the wide range of the virtual locust's jump performance. The published values from live locusts were closest to the simulated results at 8 N and were within the ranges for 5 and 15 N simulations. All simulated results shown are the average and standard deviation for that measurement for 20 *jumps* at each tension level. (1) (Bennet-Clark, 1975), (2) (Burrows and Morris, 2001), (\*) Estimate at 15 N extensor tension.